Molecular Biology of the Cell
Vol. 18, 1554–1569, May 2007

Sensory Ciliogenesis in *Caenorhabditis elegans*: Assignment of IFT Components into Distinct Modules Based on Transport and Phenotypic Profiles[D]

Guangshuo Ou,* Makato Koga,[†‡] Oliver E. Blacque,[‡§‖] Takashi Murayama,[†] Yasumi Ohshima,[†] Jenny C. Schafer,[¶] Chunmei Li,[§] Bradley K. Yoder,[¶] Michel R. Leroux,[§] and Jonathan M. Scholey*

*Center for Genetics and Development, Section of Molecular and Cellular Biology, University of California, Davis, CA 95616; [†]Department of Biology, Faculty of Sciences, Kyushu University Graduate School, 6-10-1, Hakozaki, Higashi-ku, Fukuoka 812-8581, Japan; [§]Department of Molecular Biology and Biochemistry, Simon Fraser University, Burnaby, BC V5A 1S6, Canada; [‖]School of Biomolecular and Biomedical Science, University College Dublin Conway Institute, University College Dublin, Belfield, Dublin 4, Ireland; and [¶]Department of Cell Biology, University of Alabama at Birmingham Medical Center, Birmingham, AL 35294

Submitted September 11, 2006; Revised February 2, 2007; Accepted February 7, 2007
Monitoring Editor: Erika Holzbaur

Sensory cilium biogenesis within *Caenorhabditis elegans* neurons depends on the kinesin-2–dependent intraflagellar transport (IFT) of ciliary precursors associated with IFT particles to the axoneme tip. Here we analyzed the molecular organization of the IFT machinery by comparing the in vivo transport and phenotypic profiles of multiple proteins involved in IFT and ciliogenesis. Based on their motility in wild-type and *bbs* (Bardet-Biedl syndrome) mutants, IFT proteins were classified into groups with similar transport profiles that we refer to as "modules." We also analyzed the distribution and transport of fluorescent IFT particles in multiple known ciliary mutants and 49 new ciliary mutants. Most of the latter mutants were snip-SNP mapped and one, namely *dyf-14(ks69)*, was cloned and found to encode a conserved protein essential for ciliogenesis. The products of these ciliogenesis genes could also be assigned to the aforementioned set of modules or to specific aspects of ciliogenesis, based on IFT particle dynamics and ciliary mutant phenotypes. Although binding assays would be required to confirm direct physical interactions, the results are consistent with the hypothesis that the *C. elegans* IFT machinery has a modular design, consisting of modules IFT-subcomplex A, IFT-subcomplex B, and a BBS protein complex, in addition to motor and cargo modules, with each module contributing to distinct functional aspects of IFT or ciliogenesis.

INTRODUCTION

Projecting from most eukaryotic cells, the cilium is an important microtubule (MT)-based apparatus that acts as a motile organelle and/or sensory antenna for proper cellular physiology; loss of ciliary function causes various human diseases including polycystic kidney disease, primary ciliary dyskinesia, Bardet-Biedl syndrome (BBS) and Meckel syndrome (Rosenbaum and Witman, 2002; Scholey, 2003; Pan *et al.*, 2005; Badano *et al.*, 2006; Marshall and Nonaka, 2006; Singla and Reiter, 2006). Ciliary proteins include those that are part of the axoneme, the ciliary membrane, and the matrix, as well as those required for building and maintaining the integrity of the microtubule-based organelle. Many of the latter proteins are involved in intraflagellar transport (IFT), a kinesin-2–dependent motility process in which macromolecular complexes called IFT particles deliver ciliary precursors to their site of incorporation into cilia (Kozminski *et al.*, 1993; Rosenbaum and Witman, 2002; Scholey, 2003). The nature of the components, as well as the organization and specific functions of the IFT machinery, is incompletely understood. Biochemically and genetically, IFT components are shown to include one or more kinesin-2 motors that drive anterograde transport in motility assays performed in vivo and in vitro (Cole *et al.*, 1993; Snow *et al.*, 2004; Imanishi *et al.*, 2006; Pan *et al.*, 2006), a presumptive retrograde IFT-dynein motor (Piperno *et al.*, 1998; Pazour *et al.*, 1999; Porter *et al.*, 1999; Signor *et al.*, 1999; Wicks *et al.*, 2000), and the IFT particle subcomplexes A and B (which together contain at least 6 and 11 proteins, respectively; Cole *et al.*, 1998; Baker *et al.*, 2003; Lucker *et al.*, 2005). Any one of these components could conceivably be used as an attachment point for ciliary cargo (Rosenbaum and Witman, 2002; Scholey, 2003).

To assess the role of such ciliary proteins in IFT and cilium biogenesis, we previously developed a time-lapse fluorescence microscopy assay in *C. elegans* that allows us to monitor the motility of tagged components of the IFT machinery

This article was published online ahead of print in *MBC in Press* (http://www.molbiolcell.org/cgi/doi/10.1091/mbc.E06–09–0805) on February 21, 2007.

[D] The online version of this article contains supplemental material at *MBC Online* (http://www.molbiolcell.org).

[‡] These authors contributed equally to this work.

Address correspondence to: Michel R. Leroux (leroux@sfu.ca) or Jonathan M. Scholey (jmscholey@ucdavis.edu).

Abbreviations used: IFT, intraflagellar transport; BBS, Bardet-Biedl syndrome.

in live animals (Orozco *et al.*, 1999; Signor *et al.*, 1999; Snow *et al.*, 2004; Ou *et al.*, 2005a). Time-lapse fluorescence motility assays and analyses of mutants have subsequently revealed that additional proteins participate in IFT. For example, DYF-1, DYF-3, DYF-13, and IFTA-1 are also important for ensuring the proper assembly and structural integrity of the cilium and at least in the case of DYF-1 and DYF-13, are specifically required for building the distal segment of the cilium (Blacque *et al.*, 2005; Murayama *et al.*, 2005; Ou *et al.*, 2005a,b; Blacque *et al.*, 2006). This observation is of significant interest because many cilia, including those present in vertebrate retinal cells and olfactory neurons, those of *C. elegans* amphid channel neurons, as well as those of *Chlamydomonas* engaged in mating, possess a bipartite structure (Reese, 1965; Mesland *et al.*, 1980; Perkins *et al.*, 1986). The ciliary axoneme nucleates from a transitional zone containing a basal body (modified centriole) and begins with a so-called "initial" or "middle" segment, built of doublet microtubules, and can terminate with a "distal" segment composed of singlet microtubules (see Figure 1, A and B; Perkins *et al.*, 1986). In *C. elegans*, the formation of the middle segment depends on the concerted action of two distinct kinesin-2 motors (heterotrimeric kinesin-II and homodimeric OSM-3-kinesin), whereas the assembly of the distal segment is independent of kinesin-II, requiring only the OSM-3-kinesin and associated regulators, such as DYF-1 (Snow *et al.*, 2004; Ou *et al.*, 2005a; Evans *et al.*, 2006; Pan *et al.*, 2006). The function of distal segments is unclear, but in the channel cilia they appear to be required for sensory signaling. The six known BBS proteins from *C. elegans* are bona fide IFT components that appear to mediate the interaction between the two motors and the subcomplexes A and B, but their organization within motor-IFT particle complexes and mechanism of action is poorly understood (Blacque *et al.*, 2004; Ou *et al.*, 2005a).

Although this description is satisfactory in outline, two major questions about the mechanisms of cilium biogenesis in *C. elegans* remain unanswered: 1) how is the IFT-protein machinery organized? 2) what other components are involved in anterograde and retrograde IFT, as well as cilium biogenesis? Here, we used in vivo transport assays in ciliary mutants to obtain insights into the architecture of the IFT machinery and we found that many components can be organized into several functionally specialized modules. In complementary studies, we carried out forward genetic screens to isolate novel components involved in cilium biogenesis and used positional cloning approaches to identify the molecular identity of one of them. Furthermore, based on the transport behavior of IFT-particles and ciliary structure defects in the newly and previously obtained ciliary gene mutants, they were phenotypically categorized, allowing us to also assign the encoded proteins to the IFT modules, or to specific aspects of cilium biogenesis.

MATERIALS AND METHODS

Strains and Genetic Crosses

Worms were grown on an NGM plate seeded with the *Escherichia coli* strain OP50 at 20°C using standard methods (Brenner, 1974). Wild-type (WT) *C. elegans* strains used in this work were Bristol (N2) and CB4856. Fluorescence-tagged reporters (e.g., *bbs::gfp* proteins) were crossed from WT worms to various mutant backgrounds and single-worm PCR was used to follow the mutations in each case. Deletions [*bbs-1(ok1111)* and *bbs-8(nx77)*] were detected using a single PCR reaction, where primers flanking the deletion can distinguish WT and mutant copies of the gene. Two PCR reactions detected point mutations [*osm-12(n1606)*], where one reaction preferentially amplifies the WT gene and a second reaction preferentially amplifies the mutated gene. Mutants used in this work are summarized in Tables 1 and 2. The following strains expressing green fluorescent protein (GFP) or RFP (red fluorescent protein) markers were used to mark cilium structures: amphid and phasmid channel cilia: SP2101, *osm-6(p811); mnIs17[osm-6::gfp; unc-36(+)]*; SL16, *Ex[osm-1::gfp + rol-6(su1006)]*; PT47, *Ex[che-2::gfp + rol-6(su1006)]*; OLQ cilia: CX3716, *lin-15(n765); kyIs141[osm-9::GFP5 + lin-15(+)]*; AWA cilia: CX3344, *kyIs53[odr-10::GFP]*; AWB cilia: CX3553, *lin-15(n765); kyIs104 X [str-1::GFP+ lin-15(+)]*; and AWC cilia: CX3695, *lin-15(n765); kyIs140[str-2::GFP + lin-15(+)]*; PY2417, *oyIs44[odr-1::RFP]*; AFD cilia: PY1322, *oyIs18[gcy-8::GFP]*.

The strain names of each mutant carrying the above marker are listed in Tables 1 and 2.

GFP Expression Analysis in C. elegans

Translational *gfp* fusion constructs were generated via fusion PCR as previously described (Hobert, 2002). For the translational *gfp* fusion constructs, the entire exonic and intronic sequence, along with a 5′UTR promoter fragment, was fused in-frame with *gfp*. The translational 5′UTR consisted of 536 base pairs for Y110A7A.20. Transgenic animals expressing translational *gfp* transgenes as extrachromosomal arrays in *dpy-5(e907);Ex[dpy-5(+)]* animals were generated as described previously (Ansley *et al.*, 2003).

Genetic Screen and Behavioral Assays

N2 adults were treated with EMS, and F2 progeny were screened for defects in chemotaxis assays toward NaAc or *E. coli* (OP50) lawn assay. Isolated mutants were further examined in dye-filling assays with DiI (Molecular Probes, Eugene, OR). All of the animal behavioral assays were performed as previously described (Uchida *et al.*, 2003; Murayama *et al.*, 2005). All mutants were backcrossed once with N2 animals.

Genetic Mapping and Germline Rescue

Genetic mapping was performed by the snip-SNP method (Wicks *et al.*, 2001). Genomic DNA of F35D11.11 was amplified from *dyf-14(ks69)* via PCR with a high-accuracy LA Taq polymerase (Takara, Tokyo, Japan) and purified with a QIAquick PCR purification kit (Qiagen, Chatsworth, CA). The PCR fragments were sequenced to identify the molecular lesion. YAC Y74E4 DNA was injected into the germline of *dyf-14(ks69)* for rescue.

Fluorescence Microscopy

Intraflagellar transport and cilium morphology was assayed as described previously (Snow *et al.*, 2004; Ou *et al.*, 2005a; Evans *et al.*, 2006). The fluorescent transgenic worms were anesthetized with 10 mM levamisole, mounted on agar pads, and maintained at 21°C. Images were collected using an Olympus microscope (Melville, NY) equipped with a 100×, 1.35 NA objective and an Ultraview spinning disk confocal head with excitation by a 488- argon ion laser (Perkin Elmer, Norwalk, CT). Time-lapse images were acquired at 0.3 s/frame using a cooled charge-coupled device camera (ORCA-ER; Hamamatsu, Bridgewater, NJ). Kymographs were created from the resulting stacked tiff images using Metamorph software (Universal Imaging, West Chester, PA), and the rates of fluorescent IFT particle motility along middle and distal segments were measured as described previously (Snow *et al.*, 2004).

RESULTS

Strategy for the Comprehensive Analysis of the IFT Machinery and Sensory Ciliogenesis

Our aim for this study was to analyze, as comprehensively as possible, the IFT machinery that builds the ciliated dendritic endings on ciliated neurons in the *C. elegans* nervous system (Ward *et al.*, 1975; Perkins *et al.*, 1986; Evans *et al.*, 2006) based on assays of IFT and ciliary mutant phenotypes. To begin with, we examined ciliary morphology and IFT in the various neuronal cilia of *C. elegans*, which have diverse shapes and distinct sensory functions (Figure 1; Ward *et al.*, 1975). The cilia of monociliated ASE, ASG, ASH, ASI, ASJ, ASK, and biciliated ADF and ADL neurons together form bundles of amphid channel cilia whose endings are exposed directly to the environment through openings in the cuticle, allowing them to sense water-soluble chemicals (Figure 1, A, C, D, E, G, and H; Perkins *et al.*, 1986; Perens and Shaham, 2005). By contrast, the olfactory neurons that detect volatile odorants, namely AWA, AWB, and AWC, have wing- or fan-shaped ciliated endings that are ensheathed by the adjacent sheath cells (Bargmann, 1997). Specifically, the AWA cilia form extensively branched "filaments" (Figure 1, I and M); AWB cilia form irregular "forks" with two branches of varying length (Figure 1, J and N); and AWC cilia form two

Table 1. Summary of amphid channel ciliary defects in novel dye-filling mutants

Strain	Allele	With osm-6::gfp	Genetic position		Structure[a]		IFT[b]	Other defects
			Left	Right	MS	DS		
QD8	*qj8*	KD1	X:		1	0	N	Posterior aggregation in dendrites
QD9	*qj9*	KD2	I: 1.27	I: 4.31	1	0	N	Aggregation in the cilia
QD10	*qj10*	KD3	I:		2	0	N	Aggregation at the ciliary tip
QD11	*qj11*	KD4	X:		1	0	N	Posterior aggregation in dendrites
QD12	*qj12*	KD5	X: −0.76	X: 1.84	1	0	N	Aggregation in the cilia
QD13	*qj13*							
QD14	*qj14*	KD7	I: −0.69	I: 2.94	2	2	Y	Aggregation and little IFT in the DS
QD15	*qj15*		X:					
QD16	*qj16*	KD9	II: −5.81	II: 5.5	1	0	N	Aggregation at the dendritic endings
QD17	*qj17*	KD10	I: 3.04	I: 5	2	0	N	Aggregation in the cilia
QD18	*qj18*		X: 0.44	X: 2.13				
QD19	*qj19*							
QD20	*qj20*	KD13	X:		2	1	Y	Mis-orientation of the distal segment
QD21	*qj21*	KD14	IV: −4.77	IV: 4.7	2	0	N	Aggregation in the cilia
QD22	*qj22*	KD15	III:		2	1	N	Aggregation in the cilia
QD23	*qj23*	KD16	X: −11.1	X: −1.63	2	0	Y	None
QD24	*qj24*	KD17			2	1	Y	Aggregation at the tip of the MS
QD25	*qj25*	KD18	X:		1	0	N	Posterior aggregation in dendrites
QD26	*qj26*	KD19	X:		1	0	N	Posterior aggregation in dendrites
QD27	*qj27*	KD20	X:		1	0	N	None
QD28	*qj28*	KD21	X: −6.3	X: −3.2	2	0	Y	Aggregation at the ciliary tip
QD30	*qj30*	KD23	X:		1	0	N	Aggregation in the cilia and dendrites
QD31	*qj31*	KD24	X:		1	0	N	Aggregation in the cilia
QD32	*qj32*	KD25	I: 1.27	I: 5	1	0	N	Posterior aggregation in dendrites
QD33	*qj33*	KD26	V: 1.54	V: 5.98	1	0	N	Aggregation in the cilia
QD34	*qj34*	KD27	I: 0.47	I: 3.95	1	0	N	Aggregation in the cilia
QD35	*qj35*	KD28	V: 2.55	V: 10.26	2	1	Y	None
QD36	*qj36*	KD29		IV: −3.39	0	0	N	Posterior aggregation in dendrites
QD37	*qj37*	KD30	I: 0.91	I:5	1	0	N	Aggregation in the cilia
QD38	*qj38*	KD31		X: −11.1	1	0	N	None
QD39	*qj39*	KD32		X: −11.1	1	0	N	Posterior aggregation in dendrites
QD40	*qj40*	KD33	X:		1	0	N	None
QD41	*qj41*	KD34			1	0	N	Aggregation in the cilia
QD42	*qj42*	KD35	II: −5.81	II: 1.44	0	0	N	Aggregation at the dendritic endings
QD43	*qj43*		IV:					
QD44	*qj44*		V:					
QD45	*qj45*	KD38	X: 15.42	X: 20.79	1	0	N	Posterior aggregation in dendrites
QD46	*qj46*	KD39	X:		0	0	N	None
QD47	*qj47*	KD40	IV: −7.99	IV: 1	2	0	Y	None
QD48	*qj48*	KD41	I: −5.6	I: 4.31	2	0	N	Aggregation in the cilia
QD49	*qj49*	KD42	X:		1	0	N	Posterior aggregation in dendrites
QD50	*qj50*	KD43	X:		0	0	N	Aggregation at the dendritic endings
QD51	*qj51*	KD44	I: 0.91	I: 3.95	2	1	Y	Aggregation at the tip of the MS
QD52	*qj52*		V: 1.54	V: 5.98				
QD53	*qj53*	KD46			1	0	N	Posterior aggregation in dendrites
QD54	*qj54*		V:					
QD55	*qj55*	KD48	X: 1.12	X: 9.1	2	0	Y	None
FK263	*ks69*	KD49	F35D11.11		1	0	Y	Only 1–2 cilia develop with IFT
	ks101	KD50			2	1	Y	Partial dye-filling defective

Ciliary length and IFT in amphid and phasmid cilia of the mutant animals were visualized using OSM-6::GFP.

[a] Loss of amphid ciliary structure: 2, WT-like length middle segment (MS) or distal segment (DS); 1, abnormal length middle or distal segments; and 0, the complete loss of the middle or distal segment.

[b] Intraflagellar transport assays were assigned as follows: Y, detectable IFT in the remaining middle and distal ciliary segments; N, no detectable IFT was assigned.

flattened, extended and "fan"-like sheets (Figure 1, K and O). Finally, the thermotactic AFD neuron has a short cilium and many microvilli-like projections (Figure 1, L and P; Bargmann, 1997). Among these diverse cilia subtypes, we were only able to reliably detect robust IFT in the amphid and phasmid channel cilia, where IFT particles move in a biphasic manner along the initial and distal segments of the axoneme (Snow *et al.*, 2004; Figure 1, B and F). For example, using a known fluorescent IFT-particle marker, OSM-1::GFP, IFT particles moved at 0.70 ± 0.09 μm/s (n = 105) in the initial segment and 1.18 ± 0.14 μm/s (n = 110) along the distal segment of all measured phasmid cilia. This latter finding differs from previous data (Qin *et al.*, 2005) and indicates that the coordinate action of kinesin-II and OSM-3-kinesin drives biphasic IFT particle transport in the phasmid cilia, as well as in the amphid channel cilia (Snow *et al.*,

Table 2. Summary of amphid channel ciliary defects in previously known mutants

				Amphid channel cilia				
					Structure[a]			
Gene	Allele	Genetic position	Protein	Strain	MS	DS	IFT[b]	Other defects
dyf-1	*tm2085*	I: −0.43	F54C1.5	KD239	2	0	Y	None
dyf-2	*m160*	III: 21.57 ± 0.32	ZK520.1+ZK520.3	KD8802	1	0	N	Aggregation in the cilia
dyf-3	*m185*	IV: −4.34 ± 0.106	C04C3.5	KD8803	1	0	N	posterior aggregation in dendrites
dyf-4	*m158*	V: 4.32 ± 0.293	Uncloned	KD8804	2	1	Y	Mis-orientation of the ciliary distal segment
dyf-5	*mn400*	I: 3.76	M04C9.5	KD8805	2	2	Y	Aggregation and little IFT in the distal segment
dyf-6	*m175*	X: 1.88	F46F6.4	KD8806	2	0	Y	None
dyf-8	*m539*	X: 1.45 ± 0.007	C43C3.3	KD8808	1	0	N	Aggregation in and mis-orientation of the cilia
dyf-9	*n1513*	V: 23.50 ± 0.983	Uncloned	KD8809	1	0	N	Aggregation in the cilia
dyf-10	*e1383*	I: 1.56 ± 0.043	Uncloned	KD8810	2	1	Y	Occasional aggregation in the cilia
dyf-11	*mn392*	X: −18.27 ± 0.244	Uncloned	KD8811	1	0	N	Aggregation in the transitional zone
dyf-12	*sa127*	X: 2.00 ± 0.073	Uncloned	KD246	2	1	Y	Very short distal segment and aggregation at its tip
che-2	*e1033*	X: −19.76 +/− 0.046	F38G1.1	KD67	1	0	N	posterior aggregation in dendrites
che-10	*e1809*	II: −2.62 ± 0.221	Uncloned	KD189	0	0	N	Accumulation at dendritic endings and very few cilia
che-11	*e1810*	V: 3.67 ± 0.015	C27A7.4	KD77	2	1	N	Aggregation in the cilia
che-13	*e1805*	I: 5.05 ± 0.002	F59C6.7	KD87	1	0	N	Posterior aggregation in dendrites
che-14	*e1960*	I: 0.45 ± 0.005	F56H1.1	KD190	2	1	Y	The distal segment is less intense and mis-orientated
mec-8	*e398*	I: 3.76 ± 0.001	F46A9.6	KD200	2	1	Y	Transitional zones are not at the different positions
daf-6	*e1377*	X: 21.49 ± 0.015	F31F6.5	KD186	2	2	Y	Mis-orientation of the ciliary distal segment
osm-5	*p813*	X: −12.66 ± 0.005	Y41G9A.1	KD107	1	0	N	Posterior aggregation in dendrites
unc-6	*e78*	X: −2.01 ± 0.028	F41C6.1	KD217	2	2	Y	None
unc-33	*e204*	IV: −3.68 ± 0.036	Y37E11C.1	KD218	2	2	Y	Less intense signal in the ciliary distal segment
unc-101	*m1*	I: 13.23 ± 0.052	K11D2.3	KD196	2	0	Y	Less intense signal in the ciliary middle segment
unc-104	*e1265*	II: 0.21 ± 0.005	C52E12.2	KD197	2	2	Y	None
unc-119	*ed3*	III: 5.57 ± 0.016	M142.1	KD198	2	0	Y	None

Ciliary length and IFT in amphid and phasmid cilia of the mutant animals were visualized using OSM-6::GFP except that *dyf-4* and *dyf-12* were assayed using CHE-2::GFP.

[a] Loss of amphid ciliary structure: 2, WT-like length middle segment (MS) or distal segment (DS); 1, abnormal length middle or distal segments; and 0, the complete loss of the middle or distal segment.

[b] Intraflagellar transport assays were assigned as follows: Y, detectable IFT in the remaining middle and distal ciliary segments; N, no detectable IFT was assigned.

2004). Accordingly, in the studies described below, we focused on an examination of the transport and distribution of IFT particles in the hydrophilic molecule-sensing amphids and phasmids in various known and novel ciliary mutants.

Previously Identified Mutants Implicated in Cilium Biogenesis

Work done by the *C. elegans* community has produced a valuable collection of ciliary mutants that can be used to illuminate mechanisms of IFT and ciliogenesis (Scholey, 2003; Inglis *et al.,* 2006b). For example, the existing dye-filling (*dyf*), chemotaxis-defective (*che*), osmotic avoidance–defective (*osm*), and dauer larva formation–defective (*daf*) mutants [with the exception of *osm-8(n1518*), *osm-10(n1602*), and *osm-13 (e329)*] have defective sensory cilia structure and/or function (Table 2; Starich *et al.,* 1995; Scholey *et al.,* 2004), and in addition, the mechanosensation defective mutant *mec-8* was also reported to display ciliary defects (Perkins *et al.,* 1986). Furthermore, it is possible that some of the uncoordinated (*unc*) mutant genes might also be involved in cilium biogenesis, including, for example, UNC-119, whose ortholog in *Chlamydomonas* is a POC protein (*p*roteome *o*f *c*entriole; Keller *et al.,* 2005) and whose ortholog in *Drosophila* is a cilia "compartment" protein (Avidor-Reiss *et al.,* 2004). Accordingly, we investigated IFT and ciliary structure in five Unc mutants, namely *unc-6*, *unc-33*, *unc-101*, *unc-104,* and *unc-119* mutants. In all five animals we found abnormalities of dye uptake and in *unc-101* and *unc-119* mutants the distal segments of cilia were not formed (Table 2).

Genetic Screen for Novel Components involved in Cilium Biogenesis

To identify new IFT and ciliogenesis components, we mutagenized N2 worms with ethyl-methanesulfonate (EMS) and used behavioral assays to screen for F2 mutants defective in chemotaxis toward the hydrophilic chemical, sodium

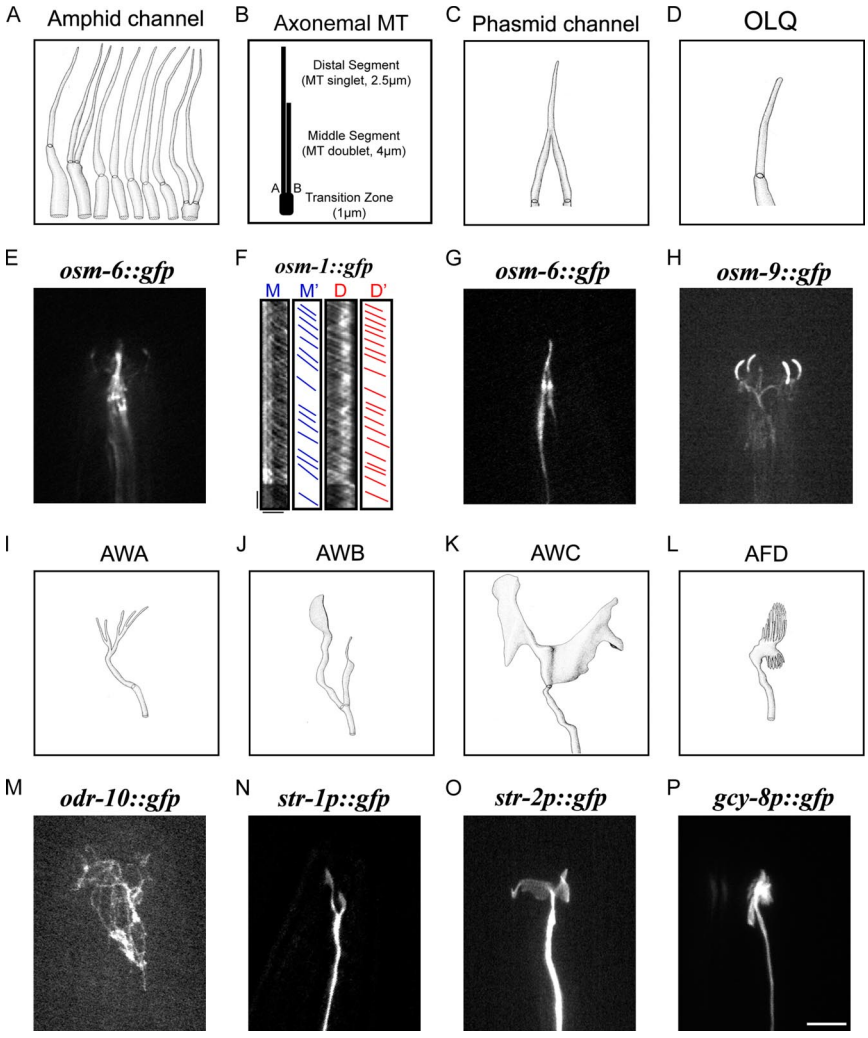

Figure 1. Schematics and fluorescence microscopy of *C. elegans* neuronal cilia. (A, C, D, I, and L) Cilia structure schematics adapted from Ward *et al.* (1975). (B) The schematic drawing of axonemal MTs in amphid channel cilia which contain 1-μm-long transitional zone, 4-μm-long middle segment with doublet MTs, and 2.5-μm-long distal segment with singlet MTs. (E, G, H, M, and P) Fluorescence microscopic images of neuronal cilia. Amphid channel cilia are ASE, ADF, ASG, ASH, ASI, ASJ, ASK, and ADL (from left to right in A); among them ADF and ADL are biciliated, and they are visualized using the distribution of an IFT-particle protein OSM-6::GFP labeled with GFP (E). Phasmid channel cilia (C) can be labeled with GFP::IFT-particle proteins such as OSM-1::GFP (F) or OSM-6::GFP (G). PHA and PHB cilia individually extend their middle segments from a transition zone, and their distal segments enter together into a phasmid pore. Intraflagellar transport in phasmid cilia displays biphasic rates (F): kymographs with corresponding schematics showing the lines representing selected OSM-1::GFP particle trajectories along the middle segments (M and M′) and the distal segments (D and D′), and motility along the distal segments is faster than along middle segments; horizontal bar, 2.5 μm and vertical bar, 5 s in F. (D and H) Outer-labial quadrant neuron (OLQ) cilia, and the GFP translational fusion of a TRPV channel protein OSM-9 marks their cylindrical shape. (I and M) The branched AWA cilia, which are marked by GFP translational fusions of a seven-span transmembrane odorant receptor, ODR-10 (M). (J and N) The "fork" shaped AWB cilia, which are visualized using a GFP transcriptional fusion of a seven-span transmembrane receptor, STR-1 (N). (K and O) The "fan"-shaped AWC cilia, which can be labeled with the transcriptional fusion of the seven-span transmembrane receptor, STR-2 (O). (L and P) "Finger"-shaped AFD cilia, which are marked by the distribution of GFP proteins driven by the promoter of a transmembrane guanylyl cyclase, GCY-8 (P). Bar, 5 μm.

acetate (NaAc) or *E. coli* food (Figure 2A). One hundred twenty-six independent NaAc chemotaxis-defective strains were isolated from 150,000 mutagenized haploid genomes, and we used dye-filling assays to identify 47 of them as being *dyf* mutants, which are likely defective in ciliary structure. We used single-nucleotide polymorphisms between Bristol N2 strain and Hawaii CB4856 strain to map the Dyf phenotype (Table 1 and Supplementary Table S1), allowing us to position 42 mutations onto specific chromosomes, with 21 of them being positioned between two genetic markers. This snip-SNP mapping data provides a good basis for further positional cloning of the novel *Dyf* mutations; for example, many of the *dyf* mutants initially identified and mapped (Starich *et al.*, 1995) were subsequently cloned (Blacque *et al.*, 2005; Murayama *et al.*, 2005; Ou *et al.*, 2005a; Bell *et al.*, 2006; Efimenko *et al.*, 2006).

Five additional mutant strains were isolated by screening ~100,000 EMS-mutagenized haploid genomes for defects in "food-orientation" *E. coli* assays. In these mutant strains, 2–8% of animals moved to an area more than 1.5 cm away from a bacterial lawn within 3 h, whereas fewer than 0.1% of WT animals did so. Among such mutants, FK247 (*ks68*) and FK263 (*ks69*) mutants displayed a Dyf phenotype, suggesting abnormal ciliary structures. *ks68* is allelic to the *che-2* gene, which is known to encode an IFT-particle B subunit homologue, IFT80, whereas we now show that *ks69* is a novel ciliary mutant that we name *dyf-14*.

We examined the distribution of the fluorescence-tagged IFT particle protein, OSM-6::GFP, in the amphid channel cilia of *dyf-14(ks69)* and observed a severe loss of cilia and abnormal IFT particle aggregates in the dendritic endings (Figure 2, B and C). Similarly, no ciliary structure was detectable in the phasmid cilia of *dyf-14(ks69)*, and the GFP signal terminates at the posterior region of the cell body (Figure 2, D and E). Given that the *dyf-14(ks69)* mutant exhibited an interesting ciliary phenotype consistent with the gene encoding a protein important for cilium biogenesis, we sought to clone *dyf-14(ks69)*. SNP mapping was first used to place *dyf-14(ks69)* within a 2.7-map unit region on chromosome II, and the germline transformation of the YAC clone Y74E4 fully rescued its Dyf phenotype. Sequencing of a predicted open reading frame (F35D11.11) of Y74E4 in *dyf-14(ks69)* animals revealed a G-to-A transition at 2210 nt, which changes 737 R to a premature stop codon. These data suggest that F35D11.11 corresponds to the *dyf-14* gene (Figure 2F). To identify its coding region, we amplified the sequences expressed by *dyf-14* cDNAs using RT-PCR. The *dyf-14* gene encodes three proteins of 1901 (DYF-14C), 1959 (DYF-14A), or

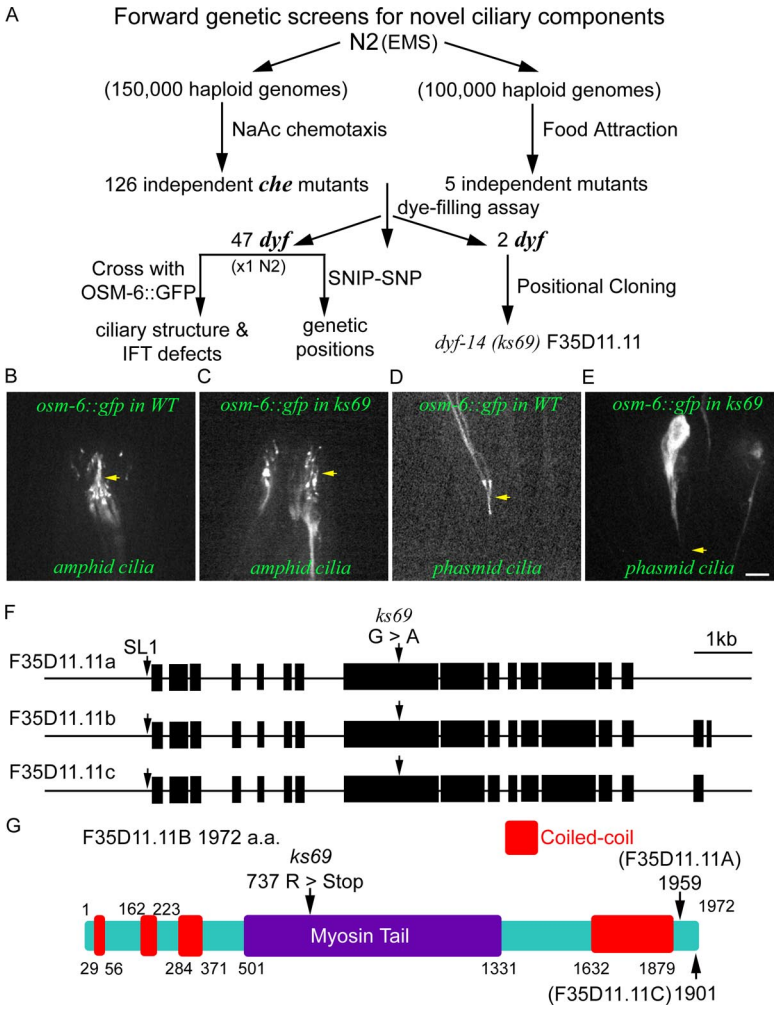

Figure 2. Identification and characterization of novel ciliary components. (A) Strategy for forward genetic screens to isolate novel ciliary components. N2 worms were mutagenized with EMS. About 150,000 haploid genomes were screened with NaAc chemotaxis assays, and 126 independent chemotaxis-defective strains were isolated; among them, 47 fail to uptake fluorescent dye. In another screen, 5 mutants were obtained from 100,000 haploid genomes based on defects in food sensation, and 2 of them were *dyf* mutants. After one backcross with N2, positional cloning approaches, including SNIP-SNP mapping and rescue experiments, were carried out to genetically map and clone these mutants. One of them, *dyf-14 (ks69)*, was cloned and bears a mutation in the gene F35D11.11. In parallel, IFT markers (OSM-6::GFP) were introduced into these mutants to detect their ciliary and IFT defects. (B–E) Ciliary structures of WT (B and D) and *dyf-14(ks69)* animals (C and E) in their amphid (B and C) and phasmid channel cilia (D and E). Arrows point to the middle-distal segment junctions. Only one or two amphid channel cilia develop and no phasmid channel cilia are visible. The dendritic endings of amphid channel neurons form aggregates, whereas there is no accumulation of OSM-6::GFP at the phasmid dendritic endings. *dyf-14(ks69)* corresponds to F35D11.11 (F) and has three transcripts spliced with SL1; the mutant possesses a G-to-A transition at 2210 nt, causing residue 737 R to mutate to a stop codon (G). The deduced DYF-14 protein contains four coiled-coil domains and one myosin-tail like domain.

1972 (DYF-14B) amino acid residues, with different C-termini (Figure 2, F and G). DYF-14 proteins contain four predicted coiled-coil regions and one myosin tail-like domain. A database search revealed that the DYF-14B protein shows sequence similarity to the conceptual translation product of a human cDNA clone, named ENSP00000357793 (E value $2.6e^{-61}$), whose involvement in cilium biogenesis is unknown.

A Modular Architecture for the IFT Protein Machinery in Amphid Channel Cilia

To examine the relative organization of most *C. elegans* IFT proteins compared with known *Chlamydomonas* ciliary protein homologues, as well as recently discovered *C. elegans* IFT-related proteins within the IFT particle, we expressed GFP-tagged versions of these proteins in *bbs* mutant backgrounds and analyzed their in vivo transport profiles. On the basis of our previous findings (Ou *et al.*, 2005a), we expected the GFP-tagged proteins to associate with either the kinesin-II/IFT-A subcomplex or the OSM-3/IFT-B subcomplex, which are dissociated in *bbs* mutants and to travel at their respective velocities of 0.5 μm/s along only the middle segment or 1.3 μm/s along the middle and distal segments. By employing this experimental approach, we have obtained an extensive set of transport profiles, which has now allowed us to present the first comprehensive description of the IFT machinery that builds *C. elegans* sensory cilia.

In addition, we have also examined the distribution and transport of a fluorescent IFT particle protein marker in the cilia of our collection of ciliary mutants. By careful comparison of the observed cilia/IFT defects with those of known cilia/IFT mutants, we assigned them to the same set of phenotypic classes. In this way, we were able to assign the known and yet-to-be-identified ciliary proteins into the following functionally specialized modules or to steps in the pathway of ciliogenesis (summarized in Figure 7).

IFT-Particle Subcomplex A and B Modules: Conveyors for Anterograde and Retrograde IFT

The IFT particles, which were first identified in *Chlamydomonas* flagellar extracts, consist of two subcomplexes, A and B (Cole *et al.*, 1998; Lucker *et al.*, 2005). These subcomplexes are thought to be capable of binding multiple cargo molecules such as ciliary structural precursors and signaling molecules and transporting them along the cilium (Rosenbaum and Witman, 2002; Scholey, 2003). Previously, we showed that in *bbs* mutants, CHE-11/IFT140 (IFT complex A) moves independently from both OSM-5/IFT88 and CHE-2/IFT80 (IFT complex B), suggesting that IFT particle A and B subcomplexes are dissociated and moved separately by kinesin-II and OSM-3-kinesin motors, respectively (Ou *et al.*, 2005a). Here, we rigorously test and extend this model by determining the transport profiles of another three known subcomplex B components (OSM-1/IFT172, CHE-13/IFT57, and

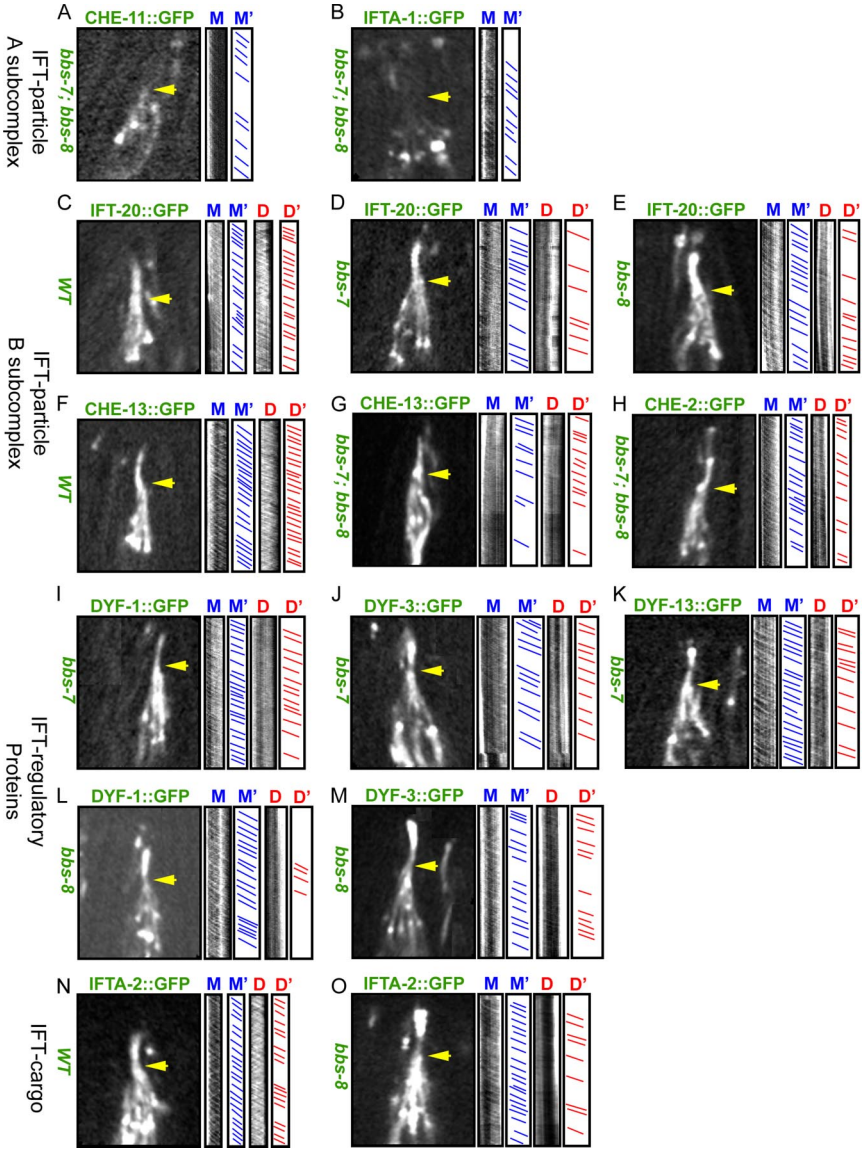

Figure 3. Transport of IFT-particle, accessory and cargo proteins in WT and *bbs* mutants. Shown are representative "still" fluorescence images and corresponding kymographs (M, middle; D, distal) and kymograph schematics (M′ and D′), obtained from the transport analysis of GFP-tagged IFT proteins in *bbs* mutant cilia. (A and B) IFT-particle subcomplex A components (CHE-11 and IFTA-1) are transported only along middle segments of *bbs-7; bbs-8* double mutant cilia at a (Kinesin-II-like) slow rate of ~0.5 μm/s. (C–H) IFT-particle subcomplex B (IFT-20, CHE-13 and CHE-2) transported along the middle (M, M′) and distal (D and D′) segments of WT (C and F) and *bbs-7*(D), *bbs-8*(E) single or *bbs-7;bbs-8* double mutant (G and H)) cilia at the (OSM-3-kinesin) fast rate of ~1.3 μm/s. (I–M) GFP-tagged DYF-1, DYF-3, and DYF-13 are transported along the middle and distal segments of *bbs* mutant cilia at the fast rates. (N and O) GFP-tagged IFTA-2, a potential cargo protein, is transported along the middle and distal segments of WT (N) and *bbs-8* mutant (O) cilia at the fast rate. Steeper lines in the kymographs correspond to slower speeds. Arrowheads denote the approximate boundary of middle and distal segments.

Y110A7A.20/IFT20) in *bbs* mutants. First, we constructed a translational GFP reporter for the nematode homolog of *Chlamydomonas* IFT20, Y110A7A.20, which has not been studied in *C. elegans*, and determined that, like other IFT particle components, IFT-20::GFP undergoes biphasic transport along the middle (~0.7 μm/s) and distal segments (~1.3 μm/s) of WT cilia (Figure 3C and Table 3). In agreement with our previous observations (Ou *et al.*, 2005a), we found that all three GFP-tagged subcomplex B proteins displayed OSM-3-kinesin–associated fast rates in the middle (~1.1 μm/s) and distal segments (~1.3 μm/s) of *bbs* mutant cilia (Figures 3, D, E, G, and H, and 4, B–D, and H, and Table 3).

DYF-3/Qilin likely functions as a subcomplex B component based on its IFT motility and mutant ciliary phenotype (Murayama *et al.*, 2005; Ou *et al.*, 2005b). Interestingly, the *C. elegans* interactome project (Li *et al.*, 2004b) uncovered a protein–protein interaction between BBS-7 and DYF-3, indicating that DYF-3 may help dock, or link, subcomplex B to the BBS protein module. As predicted by this hypothetical interaction network, we found that in *bbs* mutants, DYF-3::GFP is moved uniquely by OSM-3-kinesin along the middle and a few remaining distal segments, establishing its association with OSM-3-kinesin/subcomplex B (Figure 3, J and M, and Table 3). Verification of these interactions and uncovering additional connections between and among BBS and core/peripheral IFT proteins will necessitate a global analysis of these proteins by yeast two-hybrid and coimmunoprecipitation studies. We also note that, although DYF-3 has been found in the *Chlamydomonas* flagellar proteome, its apparent absence from the biochemically isolated IFT particle B subcomplex suggests that it may possess a more "peripheral" location or loose association within the macromolecular architecture of the IFT machinery.

Our data suggest that IFT-particle subcomplexes A and B from *C. elegans* form discrete functional modules, as they do in *Chlamydomonas*, and they describe the approximate spatial position of these modules within the IFT machinery (see Figure 7A). These findings are also consistent with numerous functional studies conducted in *C. elegans* and *Chlamydomonas*, which describe differential roles for subcomplex B in anterograde transport and subcomplex A in retrograde transport (Rosenbaum and Witman, 2002; Scholey, 2003). Loss of function of components in IFT-particle subcomplex B inhibit anterograde IFT, resulting in ~2-μm-long residual

Table 3. Transport velocities of GFP-tagged IFT proteins in WT and *bbs* mutant animals

Anterograde motility	Strain	Reference	Average velocities ($\mu m\ s^{-1}$)			
			Middle segment	N	Distal segment	N
Kinesin-2 motors						
KAP-1::GFP	*WT*	Snow *et al.* (2004)	~0.70		None	
	bbs-1		0.58 ± 0.06	107	None	
OSM-3::GFP	*WT*	Snow *et al.* (2004)	~0.70		~1.30	
	bbs-1		1.18 ± 0.16	105	1.29 ± 0.13	88
IFT particle A						
CHE-11::GFP	*WT*	Ou *et al.* (2005a)	~0.70		~1.30	
	bbs-1		0.59 ± 0.07	104	None	
	bbs-7	Ou *et al.* (2005a)	0.50–0.60		None	
	bbs-7; bbs-8		0.52 ± 0.07	109	None	
IFTA-1::GFP	*WT*	Blacque *et al.* (2006)	~0.70		~1.30	
	bbs-7; bbs-8		0.56 ± 0.08	102	None	
IFT particle B						
CHE-2::GFP	*WT*	Ou *et al.* (2005a)	~0.70		~1.30	
	bbs-1		1.02 ± 0.12	108	1.18 ± 0.15	84
	bbs-7	Ou *et al.* (2005a)	1.10–1.30		~1.30	
	bbs-7; bbs-8		1.12 ± 0.13	103	1.32 ± 0.16	83
OSM-5::GFP	*WT*	Ou *et al.* (2005a)	~0.70		~1.30	
	bbs-7	Ou *et al.* (2005a)	1.10–1.30		~1.30	
	bbs-7; bbs-8		1.11 ± 0.16	100	1.32 ± 0.14	63
CHE-13::GFP	*WT*		0.69 ± 0.09	106	1.25 ± 0.12	107
	bbs-7; bbs-8	Ou *et al.* (2005a)	1.04 ± 0.12	105	1.20 ± 0.16	74
OSM-1::GFP	*WT*		0.75 ± 0.08	108	1.30 ± 0.16	104
	bbs-1		1.10 ± 0.11	106	1.28 ± 0.15	74
	bbs-7		1.12 ± 0.13	111	1.33 ± 0.15	84
	bbs-8		1.09 ± 0.16	104	1.33 ± 0.12	75
IFT20::GFP	*WT*		0.71 ± 0.09	106	1.28 ± 0.14	107
	bbs-7		1.20 ± 0.17	105	1.33 ± 0.18	85
	bbs-8		1.15 ± 0.17	108	1.28 ± 0.18	72
Novel DYF proteins						
DYF-1::GFP	*WT*	Ou *et al.* (2005a)	~0.70		~1.30	
	bbs-7		1.15 ± 0.15	109	1.29 ± 0.14	82
	bbs-8		1.16 ± 0.12	110	1.31 ± 0.14	81
DYF-3::GFP	*WT*	Ou *et al.* (2005b)	~0.70		~1.30	
	bbs-7		1.12 ± 0.15	107	1.33 ± 0.13	74
	bbs-8		1.10 ± 0.18	103	1.31 ± 0.15	88
DYF-13::GFP	*WT*	Blacque *et al.* (2005)	~0.70		~1.30	
	bbs-7		1.08 ± 0.13	112	1.30 ± 0.12	77
IFT cargo						
IFTA-2::GFP	*WT*		0.72 ± 0.10	104	1.23 ± 0.09	105
	bbs-8		1.07 ± 0.12	102	1.29 ± 0.14	71
BBS proteins						
BBS-1::GFP	*bbs-1*		0.76 ± 0.13	110	1.33 ± 0.15	114
	bbs-7		None		None	
	bbs-8		None		None	
BBS-5::GFP	*WT*		0.73 ± 0.09	106	1.30 ± 0.15	104
	bbs-1		None		None	
	bbs-7		None		None	
	bbs-8		None		None	
BBS-7::GFP	*bbs-7*	Ou *et al.* (2005a)	~0.70		~1.30	
	bbs-8		None		None	
BBS-8::GFP	*bbs-8*	Ou *et al.* (2005a)	~0.70		~1.30	
	bbs-1		None		None	
	bbs-7		None		None	

middle segments and posterior aggregation along the dendrites (Rosenbaum and Witman, 2002; Scholey, 2003). By "phenoBLASTing" the new mutants against previously characterized ciliary mutants, we found that *dyf-9, dyf-11, qj8, qj11, aj25, qj26, qj27, qj32, qj38, qj40, qj45, qj49,* and *qj53* may function along with other components of IFT-particle subcomplex B (Figures 5, 6, and 7B and Tables 1 and 2). On the other hand, loss of function of components in IFT-particle subcomplex A block retrograde IFT driven by CHE-3, the IFT-dynein (Signor *et al.*, 1999; Wicks *et al.*, 2000). Mutations of genes encoding known subcomplex A proteins (e.g., *che-11*, *daf-10*) and likely subcomplex A–associated components (e.g., *dyf-2*, *ifta-1*) are characterized by the formation of aggregates within the remaining cilia and no, or very little IFT is detectable in these mutants (Qin *et al.*, 2001; Blacque *et al.*, 2006; Efimenko *et al.*, 2006). Here, we report that IFT-particle (OSM-6::GFP) aggregates form along sensory cilia in *qj9, qj10, qj12, qj16, qj17, qj21, qj22, qj28, qj30, qj31, qj33, qj34, qj37,*

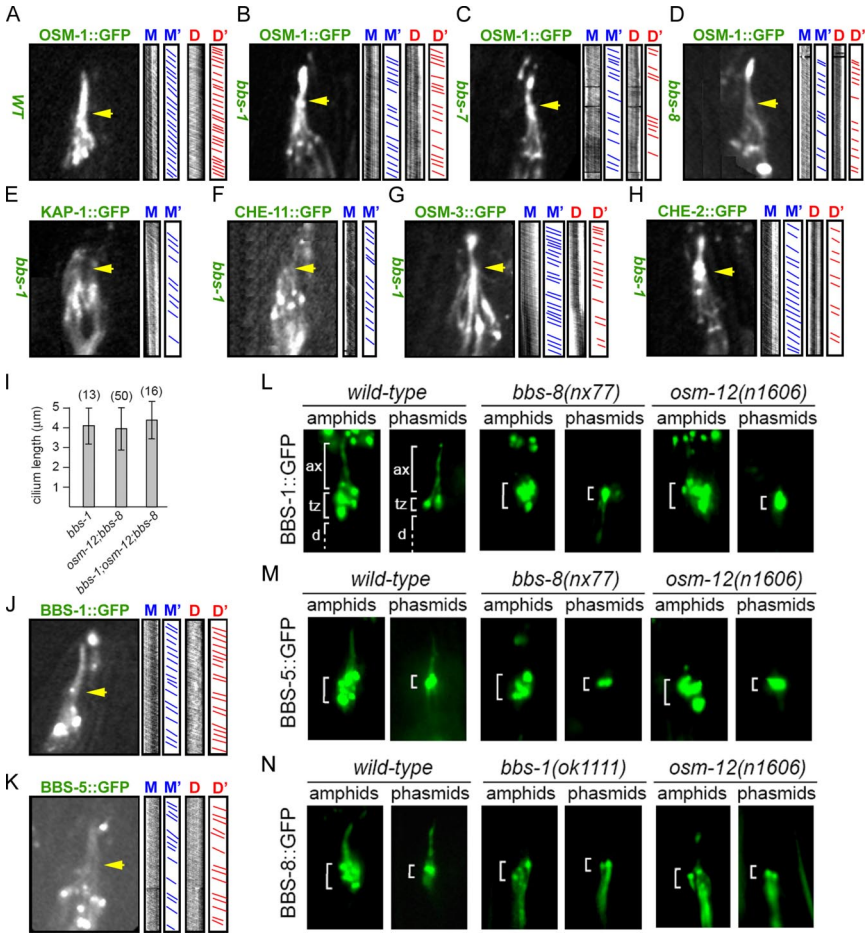

Figure 4. BBS proteins participate in IFT as functionally interdependent components of the same biological process. Shown in A–H are representative "still" fluorescence images and corresponding kymographs (M and D) and kymograph schematics (M′ and D′), obtained from the transport analyses of GFP-tagged IFT proteins along the amphid cilia of WT or *bbs* mutants. The destabilization of IFT assemblies in *bbs-1* mutants is similar to those of *bbs-7* or *bbs-8* mutants. (A–D) IFT-particle subcomplex B (OSM-1) is transported along the middle (M and M′) and distal (D and D′) segments of WT (A) and *bbs-1*, *bbs-7*, and *bbs-8* mutant (B–D) cilia, and OSM-1::GFP has the same defects in three different *bbs* mutants, namely unitary fast transport along both middle and distal segment and aggregation along sensory cilia. Images in E–H demonstrate that heterotrimeric kinesin-II (E) and CHE-11 (IFT subcomplex A; F) move only along *bbs-1* middle segments at slow rates (M and M′), whereas OSM-3-kinesin (G) and CHE-2 (IFT subcomplex B; H) move along middle (M and M′) and distal (D and D′) segments of *bbs-1* mutants at fast rates. (I) The ciliary axonemes of single, double, and triple *bbs* mutants are the same length, based on the ASER ciliary axoneme lengths (using a *gcy-5p::gfp* reporter) of *bbs-1(ok1111)*, *bbs-7(n1606);bbs-8(nx77)* and *bbs-1(ok1111);bbs-7(n1606);bbs-8(nx77)* animals. (J and K) Biphasic IFT of BBS-1::GFP (J) and BBS-5::GFP (K) along sensory cilia. BBS-1 and BBS-5 proteins undergo IFT along the middle segment at rates characteristic of kinesin-II and OSM-3-kinesin moving together, and along the distal segment at OSM-3-kinesin's own fast rate. (L–N) BBS proteins fail to enter the ciliary axonemes of *bbs* mutant cilia. Shown are fluorescence images of amphid and phasmid cilia from WT and *bbs* mutant worms, expressing the indicated *bbs::gfp* transgene (*bbs-1::gfp* in L; *bbs-5::gfp* in M; *bbs-8::gfp* in N). In contrast to WT cilia, BBS::GFP proteins fail to enter the ciliary axonemes (ax) of *bbs* mutants, although they still accumulate at the transition zones (tz, bracket). Note that the ciliary structures are similarly orientated in each panel. d, dendrite. Steeper lines in the kymographs correspond to slower speeds. Arrowheads denote the approximate boundary of middle and distal segments.

qj41, and *qj48*, which indicates that they may function together with IFT-particle A or dynein components in retrograde IFT (Figures 6 and 7B and Table 1).

In addition to the molecules that are required for retrograde IFT in general, we uncovered several components whose mutations appear to cause defects in IFT-particle recycling at specific sites, such as the distal segment tip or the junction between the middle and distal segments. For example, DYF-5, an MAPK-related serine/threonine protein kinase (Chen *et al.*, 2006) may control IFT-particle recycling because immotile OSM-6::GFP accumulates in the distal segment, whereas IFT along the middle segment persists. The tip of the middle segment is an important site for kinesin-II recycling, and *qj14*, *qj24*, and *qj51* may be specifically involved in turnaround at this site because OSM-6::GFP accumulates at the junction between the middle and distal segments of these mutants (Figures 5, 6, and 7B, and Tables 1 and 2). Further work will be required to determine the localization of the corresponding products of these candidate "turnaround" genes.

The BBS Protein Module: Stabilization of IFT Particles

BBS is a pleiotropic disorder related to defects in 12 human genes that affect basal bodies and ciliary axonemes (Ansley *et al.*, 2003; Badano *et al.*, 2006; Blacque and Leroux, 2006; Stoetzel *et al.*, 2006, 2007). One possible explanation for the oligogenic nature of BBS is that the BBS proteins may be involved in a common genetic pathway and could form a functional hetero-oligomeric complex whose subunits have interdependent functions, i.e., the function of each one depends on the proper function of all the others. The abrogation of any subunit might be predicted to disrupt the formation and conformation of the whole module, thereby preventing it from stabilizing the motor-IFT particle assembly. The availability of live cell imaging and genetics in *C. elegans* neuronal cilia makes it an appealing system to test this hypothesis.

We first compared the ciliary structural and IFT defects of a novel *C. elegans bbs-1* allele with the known *bbs* mutants to examine if all three have similar phenotypes. *bbs-1(ok1111)* possesses a deletion spanning exons 7–9, and loss of BBS-1 function causes animal behavioral abnormalities in chemotaxis and dye filling, which are known to be related to proper ciliary function (data not shown and Mak *et al.*, 2006). As in *bbs-7* and *bbs-8* mutants (Blacque *et al.*, 2004; Ou *et al.*, 2005a), abrogating the function of BBS-1 results in the separation of moving kinesin-II (KAP-1)/IFT-A (CHE-11) and OSM-3/IFT-B (CHE-2 and OSM-1) complexes (Figure 4, A–H, and Table 3). These data support the hypothesis that the BBS-1, -7, and -8 proteins are all involved in a common

Figure 5. Structural defects of amphid channel cilia in previously known dye-filling mutants. Representative images of the ciliary structures of *dyf* mutants, as visualized with GFP-labeled IFT-particle proteins (OSM-6::GFP or CHE-2::GFP). The first row demonstrates ciliary structure in WT and four other characterized mutants. Cilia in *che-11(e1810)* mutants (IFT-particle A subcomplex) contain aggregates. *osm-5(p813)*, *che-2(e1033)*, *che-13(e1805)* (IFT-particle B subcomplex) mutants only extend very short cilia. The detailed description of genotypes and structural defects are summarized in Table 2 and Figure 7. Arrows point to the middle-distal segment junctions. Bar, 5 μm.

process, and that disruption of this process leads to the destabilization of the IFT-particle. Given that the *C. elegans* BBS-1, -2, -3, -7, and -8 proteins were previously shown to undergo IFT and be bona fide IFT-related components (Blacque *et al.*, 2004; Fan *et al.*, 2004), we suspect that all BBS proteins share this common function.

To further investigate the close genetic association of the *bbs* genes, we next examined the ciliary structure and IFT in double and triple *bbs* mutants. Using IFT motility assays, we demonstrated that the transport phenotypes observed in *bbs* single mutants are exactly phenocopied in *bbs* double mutants. Specifically, we found that GFP-tagged CHE-11 (IFT subcomplex A) and IFTA-1 (IFT subcomplex A-like, C54G7.4; Blacque *et al.*, 2006) are transported only along the ciliary middle segments of *bbs-7;bbs-8* double mutants at kinesin-II's slow rate (~0.5 μm/s) and that GFP-tagged CHE-2, CHE-13, and OSM-5 (IFT subcomplex B) are transported along the *bbs-7;bbs-8* middle and distal segments at the OSM-3-kinesin–associated fast rate (~1.3 μm/s; Figure 3, A, B, G, and H, and Table 3). These data are essentially identical to those previously found in *bbs-7* or *bbs-8* single mutants (Ou *et al.*, 2005a) and demonstrate that, like the *bbs* single mutants, IFT complex A and B components are delivered separately by kinesin-II and OSM-3-kinesin, respectively, in *bbs-7;bbs-8* double mutants.

Next, we used the *gcy-5p::gfp* reporter to illuminate the ASER cilium of single, double, and triple *bbs* mutants. Using this scheme, the ASER ciliary axoneme of WT animals is measured to be ~6 μm long (Blacque *et al.*, 2004, 2005). In all examined *bbs* mutants, *bbs-1* single (4.13 ± 0.94 μm), *bbs-7;bbs-8* double (3.92 ± 1.07 μm; Blacque *et al.*, 2004) and *bbs-1;bbs-7;bbs-8* triple (4.43 ± 0.97 μm) mutants possess comparable shortened cilium phenotypes (Figure 4I). Hence, loss of function of two or even three BBS proteins does not produce any more severe defects in ciliary length than do *bbs* single mutants.

Analysis of the transport profiles of several GFP-tagged BBS proteins (BBS-1, -5, and -8) in *bbs-1*, *-7*, and *-8* mutants

Figure 6. Structural defects of amphid cilia in novel dye-filling mutants. Representative images of ciliary structures of novel *dyf* mutants, as visualized with a GFP-labeled IFT-particle protein (OSM-6::GFP). The detailed description of genotypes and structural defects in each strain are summarized in Table 1 and Figure 7. Arrows show the middle-distal segment junctions. Bar, 5 μm.

further support the hypothesis that the *C. elegans* BBS proteins possess interdependent functions. In WT animals, BBS proteins undergo biphasic IFT (Figure 4, J and K, and Table 3), but in *bbs* mutants, GFP-tagged BBS proteins accumulate at the transition zones (basal bodies) of *bbs* mutant cilia and fail to enter the ciliary axonemes or undergo IFT (Figure 4, L–N, and Table 3). These data indicate that the function of individual BBS proteins depends on the proper function of other BBS proteins. Importantly, this phenotype is strikingly different from that observed with other IFT markers in that subcomplex A and B components can still enter the cilium in all examined *bbs* mutants (Figure 3, A–H; Blacque *et al.*, 2004, 2005; Ou *et al.*, 2005a). This indicates that the BBS proteins likely operate in the same process by forming a functional, hetero-oligomeric module that is associated with, but acts independent of, the IFT particle A and B subcomplexes (Figure 7A). Consequently, removal of a single BBS protein disrupts the assembly/conformation of the entire BBS module, thereby preventing its incorporation into the motor-IFT particle assembly and resulting in the destabilization and dissociation of the two kinesin motors with their associated IFT subcomplexes.

Accessory Motor Module: Ciliary Distal Segment Assembly for Cilium-based Signaling

In certain cilia, such as those found in *C. elegans* sensory neurons, the canonical pathway appears to be modulated by

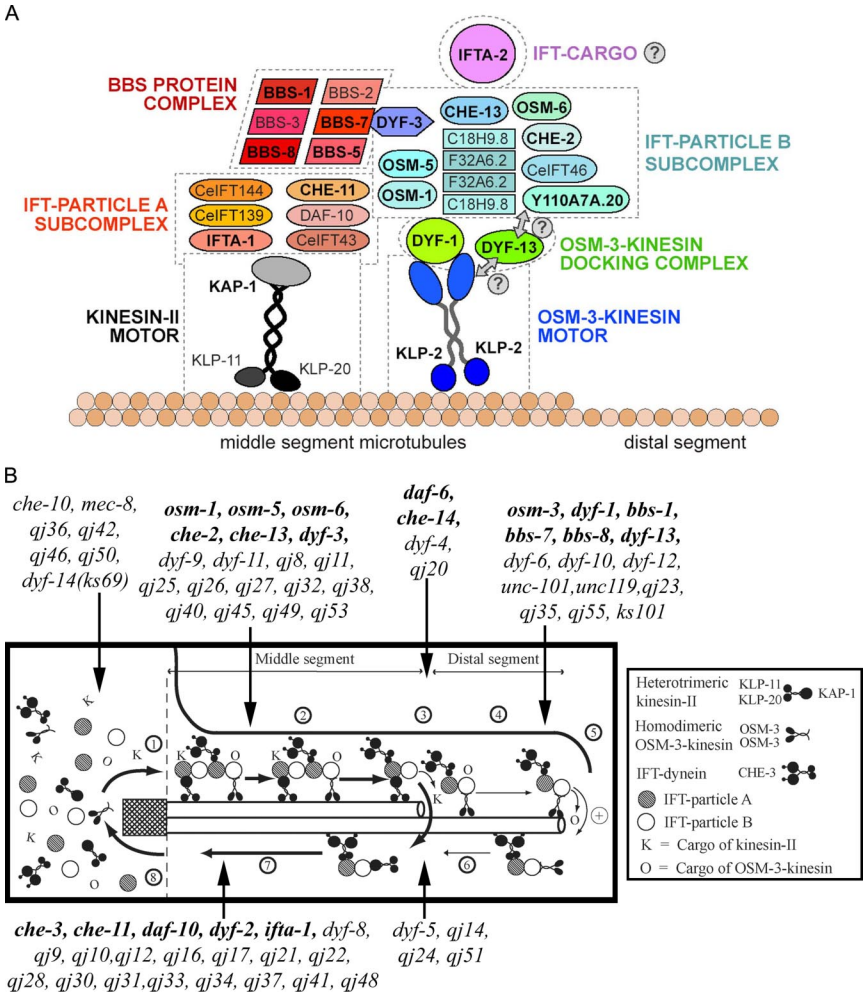

Figure 7. Modular architecture of the IFT-protein machine and molecular framework for cilium biogenesis in *C. elegans*. (A) Model of the modular architecture of the *C. elegans* IFT-protein machine. Bolded IFT proteins denote those for which data were obtained in the present study. IFT-particle modules: In *C. elegans*, IFT-particle A and B subcomplex modules are transported by both kinesin-II and OSM-3-kinesin along the middle segment of sensory cilia. Shown are the known nematode homologues of *Chlamydomonas* IFT particle components (Scholey *et al.*, 2004), including C18H9.8 (IFT74/72) and F32A6.2 (IFT81), which were previously reported to form a stable tetramer within *Chlamydomonas* IFT subcomplex B (Lucker *et al.*, 2005). IFTA-1 is an IFT-particle A subcomplex-like protein (Blacque *et al.*, 2006). Note that for those *Chlamydomonas* IFT particle components whose sequences have not yet been reported (IFT43, -139, -144, and -27), the presumed nematode homologues are designated with Ce prefixes. Accessory motor module: DYF-1, and possibly DYF-13, form a module required to activate the OSM-3-kinesin motor and/or it onto the IFT particle subcomplex B module. The exact relationship DYF-13 has with subcomplex B and the OSM-3 motor is unclear. BBS module: BBS proteins form a module that stabilizes IFT-particle A and B subcomplexes, and their interactions may be mediated via DYF-3. Cargo modules: the IFT-protein machinery delivers modules made up of various potential cargos, possibly including IFTA-2, which is associated with the IFT subcomplex B module. (B) The molecular framework forms two sequential IFT pathways to build *C. elegans* amphid channel cilia. The IFT machinery assembles at the transition zone at the base of the cilium (1). Kinesin-II and OSM-3 move the same IFT particles along the middle segments doublets (2). At the tip of the middle segment the IFT particles reorganize, kinesin-II undergoes "turnaround" (3) and it, together with its IFT particles are recycled by IFT-dynein (7). OSM-3-kinesin alone moves from the middle segment tip along the distal segment to the tip (4), where it undergoes turnaround (5) and is recycled by IFT-dynein (6) and (7). We speculate that both kinesin-2 motors redundantly deliver cargo (K and O) that stabilize the middle segment but OSM-3-kinesin alone delivers a cargo (O) that builds and stabilizes the distal singlets. Numerous proteins contribute to different steps of this process (known components in bold) and many mutations cause defects in amphid channel ciliogenesis. Details are in the text.

an accessory anterograde motor, OSM-3-kinesin (the nematode homolog of human KIF17), which cooperates with heterotrimeric kinesin-II to build middle segments, but is solely responsible for building the distal segments of cilia (Snow *et al.*, 2004; Evans *et al.*, 2006). Recently, we found that DYF-1 is required to dock OSM-3-kinesin onto IFT particles, because loss of DYF-1 function results in the abrogation of OSM-3 motor activity and a loss of distal segment structure (Ou *et al.*, 2005a). Interestingly, another IFT protein, DYF-13, also appears to function specifically in building the distal segments of cilia (Blacque *et al.*, 2005). Taken together, these data suggest that DYF-1 and DYF-13 may form a module that functions in association with OSM-3-kinesin to build distal segments. Accordingly, we predict that DYF-1 and DYF-13 will display the same transport profile as OSM-3-kinesin along *bbs* mutant cilia. When examined in *bbs-7* and *bbs-8* mutant animals, we observed that, similar to OSM-3::GFP, GFP-tagged DYF-1 and DYF-13 move along both the middle and distal segments at ~1.3 μm/s, suggesting that these DYF proteins are closely associated with, and may bind to, OSM-3-kinesin (Figure 3, I, K, and L, and Table 3).

One intriguing puzzle concerning the accessory motor module is how the DYF-1 protein docks and activates OSM-3-kinesin, given that no physical interaction can be detected between them and that DYF-1 does not directly activate OSM-3-kinesin in a single-molecule motility assay (Ou *et al.*, 2005a; Imanishi *et al.*, 2006). We proposed that DYF-1 might function with additional and unidentified molecules to form a docking complex for OSM-3-kinesin's docking and activation. One obvious implication is that our forward genetic screen may uncover novel mutants defective in this docking complex that would be expected to phenocopy *osm-3* or *dyf-1* or *dyf-13* by displaying a specific loss of the ciliary distal segment. We isolated three such mutants, namely *qj23*, *qj47*, and *qj55*. snip-SNP mapping data suggest that *qj23* and *qj55* are novel components required for the assembly of the distal segment because neither of these alleles map to the same genetic loci as *osm-3* or *dyf-1*or *dyf-13*. Accordingly, we have classified *qj23* and *qj55* as new Dyf alleles, namely *dyf-15* and *dyf-16*, respectively. In contrast, *qj47* maps to the same region as *osm-3*, and a null allele of *osm-3(p802)* fails to complement *qj47*, suggesting that *qj47* is a new allele of *osm-3* (Figures 6 and 7B and Table 1). Our set of 49 new Dyf mutants also

contains partial *dyf* mutants. For example, *ks101* does not develop any distal segments in a small subset of chemosensory neurons. It is therefore difficult to determine if this gene is specifically involved in the distal segment pathway or if it is a hypomorph, for which more severe loss-of-function alleles and molecular cloning may be needed.

We identified several other known mutants that might be involved in ciliary distal segment assembly (Figures 5 and 7B and Table 2). *dyf-6* has been recently cloned and it was reported that it has a very short middle segment without any visible IFT, suggesting that it functions as an IFT-particle B component (Bell *et al.*, 2006). However, we found that *dyf-6(m175)* only loses its distal segment and IFT still persists in the middle segment. Similarly, UNC-101 and UNC-119 are necessary for distal segment assembly, and their mutation causes the complete loss of the distal segment, with IFT still continuing in the residual middle segment. In addition, we noticed that *dyf-10, dyf-12,* and *qj35* have full-length middle segments and shorter distal segments. IFT persists in all of their middle segments, and in the remaining distal segments of *dyf-10* and *qj35*, IFT is detectable, whereas small aggregations form at the distal tip of *dyf-12* (Figures 5, 6, and 7B and Tables 1 and 2). Molecular cloning of the genes corresponding to these mutations will provide critical insights into the functions of the corresponding gene products in building the ciliary distal tips.

Finally, our genetic screen suggests that that the proper assembly of ciliary distal segments may depend on molecules other than components of the accessory motor module. The distal segment follows a linear trajectory along the channel to the amphid pore where it contacts the environment. *daf-6* and *che-14* were previously shown to be required for this linear orientation because in *daf-6* and *che-14* mutants the distal segment trajectories deviate into the adjacent sheath cells (Perens and Shaham, 2005); interestingly, we observe that *dyf-4* and *qj20* display a similar phenotype (Figures 5, 6, and 7B and Tables 1 and 2). It is notable that IFT persists in the cilia of these mutants allowing the distal segment to assemble. Thus, *dyf-4* and *qj20* might function together with *daf-6* in the sheath cells to control proper distal segment orientation.

IFT Cargo

Arguably the most poorly characterized proteins associated with the IFT machinery are the cargo molecules that are delivered into the cilia to enable cilium biogenesis and function. Candidate cargo molecules likely include structural components of the ciliary axoneme, membrane, and matrix, as well as the signaling and regulatory molecules that underlie cilia function (e.g., sensory reception). With the possible exception of radial spoke proteins and the TRPV Ca^{2+} channels, OSM-9 and OCR-2 (Qin *et al.*, 2004, 2005), no bona fide IFT cargo components have been identified and functionally characterized. However, IFTA-2 (T28F3.6), a RAB-like protein that undergoes IFT, may represent another IFT cargo (or cargo-docking) component, because this protein appears to function as a vesicle-associated signaling molecule required for the function of cilia but not for the function of the motor-IFT machinery (Schafer *et al.*, 2006). Interestingly, we show here that in WT animals, IFTA-2::GFP undergoes biphasic IFT, exactly like other IFT-particle proteins, but in *bbs-8* mutants, it undergoes transport along the middle (~1.1 μm/s) and distal (~1.3 μm/s) ciliary segments at rates characteristic of OSM-3 (Figure 3, N and O, and Table 3). This indicates that an IFTA-2–associated cargo module may associate peripherally with IFT subcomplex B and OSM-3-kinesin and may be the first indication of a docking site of cargo protein(s) on the motor-IFT machinery (Figure 7A).

Cilium Initiation

The loss of function of basal body or ciliary axoneme components could inhibit the initiation of sensory cilia, and we found seven mutations that are defective in ciliary initiation (Figure 5, 6, and 7B and Table 1 and 2). For example, there is no detectable OSM-6::GFP in the presumptive ciliary region of *qj36, qj42, qj50*, whereas in *qj46*, OSM-6::GFP forms bright dots in the ciliary region. *Che-10* (Perkins *et al.*, 1986) and *dyf-14* appear to have less severe defects in cilium initiation per se, and both of them can form one or two short cilia, whereas other cilia do not develop at all. Interestingly, in the remaining cilia of *dyf-14*, IFT is detectable, whereas no IFT is visible in the residual cilia of *che-10*. Unlike the above mutants, *mec-8* does not have defects in cilium initiation per se, but the positioning of the transition zones is dispersed rather than being tightly juxtaposed to the cilium base as in WT. This suggests that MEC-8 is involved in the positioning of the transition zone.

DISCUSSION

In the current study we used transport assays and phenotypic profiling to characterize the role of several known and novel genes and their products in IFT and cilium biogenesis and to provide the most comprehensive picture so far available of the components involved in *C. elegans* IFT and sensory ciliogenesis. The results are consistent with the *C. elegans* machinery being organized into distinct modules with specialized functions in cilium biogenesis.

Systematic approaches including proteomics and comparative genomics have recently been used to identify ciliary components (Gherman *et al.*, 2006; Inglis *et al.*, 2006a). Human primary culture respiratory epithelial cilia, *Chlamydomonas* and trypanosome flagella were isolated and their protein composition was analyzed by protein sequencing (Ostrowski *et al.*, 2002; Pazour *et al.*, 2005; Broadhead *et al.*, 2006). Comparative genomics yielded candidate ciliary components by comparisons of the genomic differences between ciliated and nonciliated organisms or the expression pattern change in ciliated and nonciliated cells or during cilium regeneration (Avidor-Reiss *et al.*, 2004; Li *et al.*, 2004a; Blacque *et al.*, 2005; Efimenko *et al.*, 2005; Keller *et al.*, 2005; Kunitomo *et al.*, 2005). Forward genetic studies provide a useful complementary method to these powerful systematic tools for identifying ciliogenesis components.

This latter approach is justified by our identification of a new protein required for cilium biogenesis, namely DYF-14. The function of this protein was previously unknown except that the human protein homolog, trichohyalin, has been reported to associate with a hair follicle intermediate filament (Rothnagel and Rogers, 1986; Fietz *et al.*, 1993), but ciliary functions were not reported previously. Protein domain analysis of DYF-14 uncovered four coiled-coil domains and one "myosin tail-like" domain. Interestingly, several components of the IFT-particle B subcomplex have coiled-coil domains including IFT81, IFT74/72, IFT57/55, and IFT20 (Cole, 2003), which may mediate protein–protein interactions (Lucker *et al.*, 2005) so DYF-14 might assemble into a protein complex, possibly the IFT-particle, that is required for ciliogenesis. More work on the expression pattern, cellular localization, and dynamics of DYF-14 is needed to determine how it functions in cilium biogenesis in *C. elegans*.

Our use of transport assays of ciliary proteins provides the most detailed model yet of the modular architecture of the

IFT machinery. In the resulting model, IFT depends on a network of dozens of interacting IFT proteins organized into modules that may execute distinct subprocesses in the assembly and maintenance of cilia (Figure 7A). BBS proteins appear to function interdependently in the same IFT-related genetic pathway, consistent with them forming a heteromeric multiprotein complex that stabilizes IFT-particle subcomplexes A and B. Two known IFT subcomplex A proteins studied (CHE-11 and IFTA-1) associate with the heterotrimeric kinesin-II motor, whereas all the known IFT subcomplex B proteins that were examined (CHE-2, CHE-13, OSM-1, OSM-5, OSM-6, IFT-20) are in close proximity to the homodimeric OSM-3-kinesin motor.

Three recently identified but relatively uncharacterized IFT regulators, DYF-1, DYF-3, and DYF-13, appear to be positioned close to OSM-3-kinesin/IFT subcomplex B. Although DYF-1 and DYF-13 associate with OSM-3-kinesin in the same manner as IFT subcomplex B, we propose they form a separate functional module, because their disruption produces overlapping phenotypes that differ from that of IFT subcomplex B mutants. Specifically, *dyf-1* and *dyf-13* mutants possess intact middle segments and loss of DYF-1 function specifically affects the function of the OSM-3-kinesin motor (Blacque *et al.,* 2005; Ou *et al.,* 2005a). Further studies are needed to uncover the specific functions of DYF-1 and DYF-13 in relation to their association with OSM-3-kinesin/subcomplex B. It is possible that these two proteins exert their distal segment-specific functions at a position that is peripheral to IFT subcomplex B, yet in close proximity with OSM-3-kinesin (Figure 7A).

In our forward genetic screens, we identified additional components that appear to function in the OSM-3-kinesin–dependent distal segment pathway. For example, *dyf-15(qj23)* and *dyf-16(qj55)* display a specific loss of the complete distal segment and their unique phenotypes suggest that the corresponding gene products could be novel components that function with DYF-1 and DYF-13 in OSM-3-kinesin docking and activation. Alternatively, they may be cargo molecules required for distal segment assembly. Careful characterization of the IFT of all available markers and gene cloning will be necessary to distinguish these possibilities. Of note is the fact that both DYF-1 and DYF-13 have homologues in other ciliated organisms, suggesting that their functions are conserved in IFT pathways of different species (Blacque *et al.,* 2005; Ou *et al.,* 2005a).

Although very poorly characterized, it is thought that numerous cargo "modules" may associate peripherally with the IFT machinery. Cargo proteins are likely to display functional properties and dynamics that are distinct from those of the integral IFT machinery (e.g., IFT-particle subunits and BBS proteins) yet even this aspect of IFT-cargo is poorly understood. For example, although the "core" IFT machinery displays persistent movement back and forth between the basal body and the distal tip of the cilium, once a cargo molecule has accumulated in the appropriate ciliary compartment, there may be a significant temporal delay before it gets recycled to the cell body by retrograde transport, and it is possible that the disruption of cargo proteins will affect cilia function without directly affecting IFT motility or the integrity of motor-IFT particle assemblies. Our present work and the findings of Schafer *et al.* (2006) on IFTA-2 suggests that it may represent cargo or likely be required for cargo association with the IFT-particle, because it is required for ciliary function but not for ciliary structure or IFT. Clearly, further work is required to identify and better characterize the cargo of the IFT machinery.

Obviously some of the proteins identified in our forward genetic screen may not be components of IFT modules, but instead they may function at different sites to control IFT and ciliogenesis. Examples include proteins involved in turnaround of the IFT machinery at the tips of the middle or distal segments (e.g., *qj14*), in transition zone positioning (e.g. *mec-8*), and in distal segment orientation (e.g., *dyf-4*) (see Figure 7B). Indeed some of the corresponding gene products may function outside of ciliated sensory neurons, for example in the surrounding sheath or socket cells (e.g., daf-6, [Perens *et al.,* 2005]). Further cloning and characterization of these genes, including tagging, localizing and studying transport of their products, may provide novel insights into the mechanisms of sensory ciliogenesis in *C. elegans* neurons.

Axon outgrowth was previously shown to be defective in ciliary mutants, indicating that sensory activity is required for sensory axon development (Peckol *et al.,* 1999). We studied cilium biogenesis in mutants defective in axon guidance (*unc-6*), axon outgrowth (*unc-33*), and axon transport (*unc-104*), and their cilia appear to be properly formed (Figure 5 and Table 2), indicating that abnormal axonal structure and function do not affect cilium biogenesis. In addition, we characterized the ciliary phenotypes of another two *Unc* mutants, *unc-101* and *unc-119*. Both of them have defective dye-filling phenotypes, and loss of their ciliary distal segments (Figures 5 and 7B and Table 2). UNC-101 is the AP-1 mu1 clathrin adaptor and mediates polarized dendritic transport of odorant receptors to olfactory cilia (Dwyer *et al.,* 2001). UNC-119 encodes a highly conserved protein required for proper development of the nervous system, and its *Chlamydomonas* ortholog is a centriole protein (Maduro and Pilgrim, 1995; Maduro *et al.,* 2000). Further work on the cellular localization and dynamics of UNC-101 and UNC-119 is necessary to explain how they function in cilium biogenesis.

Although our work provides a useful description of the protein machinery involved in sensory ciliogenesis in *C. elegans*, further work will be needed to better characterize the architecture and function of the individual modules. For example, efforts must be directed toward extending and improving the identification of cargo and regulatory molecules associated with IFT particles, and in directly testing predictions of the current model (Figure 7) by physical binding assays and structural studies. Nevertheless, the work described here should provide a framework for studying the functional hierarchy of the IFT machinery, which in turn may eventually illuminate the temporal dynamics of its assembly. In addition, by correlating the IFT motility signatures described here with phenotypic profiles of IFT components and biochemical analyses of direct physical interactions between IFT proteins, it should be possible to develop network models of the modular IFT machinery, analogous to those developed for the protein machinery involved in embryogenesis (Gunsalus *et al.,* 2005). Taken together, our work on known and novel ciliary mutants, based on in vivo assays of the transport and distribution of functional GFP fusion proteins, complements the pioneering biochemical studies done elsewhere (Cole *et al.,* 1998; Piperno *et al.,* 1998; Lucker *et al.,* 2005) and provides the first comprehensive picture and modular description of the IFT machinery that builds *C. elegans* sensory cilia.

ACKNOWLEDGMENTS

We thank T. Stiernagle and the *C. elegans* gene-knockout consortium for providing strains. Work in the Scholey laboratory is supported by National

Institutes of Health Grant GM50718. Support was from Japan Science and Technology Corporation research grant PREST to M.K. M.R.L. holds Michael Smith Foundation for Health Research (MSFHR) and CIHR scholar awards and was supported by the Canadian Institutes of Health Research (CIHR) Grant CBM134736 and the March of Dimes (equal funding from grants to M.R.L.). O.E.B. was supported by a MSFHR fellowship.

REFERENCES

Ansley, S. J. *et al.* (2003). Basal body dysfunction is a likely cause of pleiotropic Bardet-Biedl syndrome. Nature *425*, 628–633.

Avidor-Reiss, T., Maer, A. M., Koundakjian, E., Polyanovsky, A., Keil, T., Subramaniam, S., and Zuker, C. S. (2004). Decoding cilia function: defining specialized genes required for compartmentalized cilia biogenesis. Cell *117*, 527–539.

Badano, J. L., Mitsuma, N., Beales, P. L., and Katsanis, N. (2006). The ciliopathies: an emerging class of human genetic disorders. Annu. Rev. Genom. Hum. Genet. *7*, 125–148.

Baker, S. A., Freeman, K., Luby-Phelps, K., Pazour, G. J., and Besharse, J. C. (2003). IFT20 links kinesin II with a mammalian intraflagellar transport complex that is conserved in motile flagella and sensory cilia. J. Biol. Chem. *278*, 34211–34218.

Bargmann, C.a.M.I. (1997). Chemotaxis and thermotaxis. In: *C. elegans* II, ed. T.B.D.L. Riddle, B. J. Meyer, and J. R. Priess, Cold Spring Harbor, NY: Cold Spring Harbor Laboratory Press, 717–737.

Bell, L.R., Stone, S., Yochem, J., Shaw, J. E., and Herman, R. K. (2006). The molecular identities of the *Caenorhabditis elegans* intraflagellar transport genes dyf-6, daf-10 and osm-1. Genetics *173*, 1275–1286.

Blacque, O. E., and Leroux, M. R. (2006). Bardet-Biedl syndrome: an emerging pathomechanism of intracellular transport. Cell Mol. Life Sci. *63*, 2145–2161.

Blacque, O. E., Li, C., Inglis, P. N., Esmail, M. A., Ou, G., Mah, A. K., Baillie, D. L., Scholey, J. M., and Leroux, M. R. (2006). The WD repeat-containing protein, IFTA-1, is required for retrograde intraflagellar transport. Mol. Biol. Cell *17*, 5053–5062.

Blacque, O. E. *et al.* (2005). Functional genomics of the cilium, a sensory organelle. Curr. Biol. *15*, 935–941.

Blacque, O. E. *et al.* (2004). Loss of *C. elegans* BBS-7 and BBS-8 protein function results in cilia defects and compromised intraflagellar transport. Genes Dev. *18*, 1630–1642.

Brenner, S. (1974). The genetics of *Caenorhabditis elegans*. Genetics *77*, 71–94.

Broadhead, R., Dawe, H. R., Farr, H., Griffiths, S., Hart, S. R., Portman, N., Shaw, M. K., Ginger, M. L., Gaskell, S. J., McKean, P. G., and Gull, K. (2006). Flagellar motility is required for the viability of the bloodstream trypanosome. Nature *440*, 224–227.

Chen, N. *et al.* (2006). Identification of ciliary and ciliopathy genes in *Caenorhabditis elegans* through comparative genomics. Genome Biol. *7*, R126.

Cole, D. G. (2003). The intraflagellar transport machinery of *Chlamydomonas reinhardtii*. Traffic *4*, 435–442.

Cole, D. G., Chinn, S. W., Wedaman, K. P., Hall, K., Vuong, T., and Scholey, J. M. (1993). Novel heterotrimeric kinesin-related protein purified from sea urchin eggs. Nature *366*, 268–270.

Cole, D. G., Diener, D. R., Himelblau, A. L., Beech, P. L., Fuster, J. C., and Rosenbaum, J. L. (1998). Chlamydomonas kinesin-II-dependent intraflagellar transport (IFT): IFT particles contain proteins required for ciliary assembly in *Caenorhabditis elegans* sensory neurons. J. Cell Biol. *141*, 993–1008.

Dwyer, N. D., Adler, C. E., Crump, J. G., L'Etoile, N. D., and Bargmann, C. I. (2001). Polarized dendritic transport and the AP-1 mu1 clathrin adaptor UNC-101 localize odorant receptors to olfactory cilia. Neuron *31*, 277–287.

Efimenko, E., Blacque, O. E., Ou, G., Haycraft, C. J., Yoder, B. K., Scholey, J. M., Leroux, M. R., and Swoboda, P. (2006). *Caenorhabditis elegans* DYF-2, an ortholog of human WDR19, is a component of the IFT machinery in sensory cilia. Mol. Biol. Cell *17*, 4801–4811.

Efimenko, E., Bubb, K., Mak, H. Y., Holzman, T., Leroux, M. R., Ruvkun, G., Thomas, J. H., and Swoboda, P. (2005). Analysis of xbx genes in *C. elegans*. Development *132*, 1923–1934.

Evans, J. E., Snow, J. J., Gunnarson, A. L., Ou, G., Stahlberg, H., McDonald, K. L., and Scholey, J. M. (2006). Functional modulation of IFT kinesins extends the sensory repertoire of ciliated neurons in *Caenorhabditis elegans*. J. Cell Biol. *172*, 663–669.

Fan, Y. *et al.* (2004). Mutations in a member of the Ras superfamily of small GTP-binding proteins causes Bardet-Biedl syndrome. Nat. Genet. *36*, 989–993.

Fietz, M. J., McLaughlan, C. J., Campbell, M. T., and Rogers, G. E. (1993). Analysis of the sheep trichohyalin gene: potential structural and calcium-binding roles of trichohyalin in the hair follicle. J. Cell Biol. *121*, 855–865.

Gherman, A., Davis, E. E., and Katsanis, N. (2006). The ciliary proteome database: an integrated community resource for the genetic and functional dissection of cilia. Nat. Genet. *38*, 961–962.

Gunsalus, K. C. *et al.* (2005). Predictive models of molecular machines involved in *Caenorhabditis elegans* early embryogenesis. Nature *436*, 861–865.

Hobert, O. (2002). PCR fusion-based approach to create reporter gene constructs for expression analysis in transgenic *C. elegans*. Biotechniques *32*, 728–730.

Imanishi, M., Endres, N. F., Gennerich, A., and Vale, R. D. (2006). Autoinhibition regulates the motility of the *C. elegans* intraflagellar transport motor OSM-3. J. Cell Biol. *174*, 931–937.

Inglis, P. N., Boroevich, K. A., and Leroux, M. R. (2006a). Piecing together a ciliome. Trends Genet. *22*, 491–500.

Inglis, P. N., Ou, G., Leroux, M. R., and Scholey, J. M. (2006b). The sensory cilia of *Caenorhabditis elegans*. ed. WormBook, The *C. elegans* Research Community, WormBook, doi/10.1895/wormbook. 1.126.1, http://www.wormbook.org.

Keller, L. C., Romijn, E. P., Zamora, I., Yates, J. R., 3rd, and Marshall, W. F. (2005). Proteomic analysis of isolated chlamydomonas centrioles reveals orthologs of ciliary-disease genes. Curr. Biol. *15*, 1090–1098.

Kozminski, K. G., Johnson, K. A., Forscher, P., and Rosenbaum, J. L. (1993). A motility in the eukaryotic flagellum unrelated to flagellar beating. Proc. Natl. Acad. Sci. USA *90*, 5519–5523.

Kunitomo, H., Uesugi, H., Kohara, Y., and Iino, Y. (2005). Identification of ciliated sensory neuron-expressed genes in *Caenorhabditis elegans* using targeted pull-down of poly(A) tails. Genome Biol. *6*, R17.

Li, J. B. *et al.* (2004a). Comparative genomics identifies a flagellar and basal body proteome that includes the BBS5 human disease gene. Cell *117*, 541–552.

Li, S. *et al.* (2004b). A map of the interactome network of the metazoan *C. elegans*. Science *303*, 540–543.

Lucker, B. F., Behal, R. H., Qin, H., Siron, L. C., Taggart, W. D., Rosenbaum, J. L., and Cole, D. G. (2005). Characterization of the intraflagellar transport complex B core: direct interaction of the IFT81 and IFT74/72 subunits. J. Biol. Chem. *280*, 27688–27696.

Maduro, M., and Pilgrim, D. (1995). Identification and cloning of unc-119, a gene expressed in the *Caenorhabditis elegans* nervous system. Genetics *141*, 977–988.

Maduro, M. F., Gordon, M., Jacobs, R., and Pilgrim, D. B. (2000). The UNC-119 family of neural proteins is functionally conserved between humans, *Drosophila* and *C. elegans*. J. Neurogenet. *13*, 191–212.

Mak, H. Y., Nelson, L. S., Basson, M., Johnson, C. D., and Ruvkun, G. (2006). Polygenic control of *Caenorhabditis elegans* fat storage. Nat. Genet. *38*, 363–368.

Marshall, W.F., and Nonaka, S. (2006). Cilia: tuning in to the cell's antenna. Curr. Biol. *16*, R604–R614.

Mesland, D. A., Hoffman, J. L., Caligor, E., and Goodenough, U. W. (1980). Flagellar tip activation stimulated by membrane adhesions in *Chlamydomonas* gametes. J. Cell Biol. *84*, 599–617.

Murayama, T., Toh, Y., Ohshima, Y., and Koga, M. (2005). The dyf-3 gene encodes a novel protein required for sensory cilium formation in *Caenorhabditis elegans*. J. Mol. Biol. *346*, 677–687.

Orozco, J. T., Wedaman, K. P., Signor, D., Brown, H., Rose, L., and Scholey, J. M. (1999). Movement of motor and cargo along cilia. Nature *398*, 674.

Ostrowski, L. E., Blackburn, K., Radde, K. M., Moyer, M. B., Schlatzer, D. M., Moseley, A., and Boucher, R. C. (2002). A proteomic analysis of human cilia: identification of novel components. Mol. Cell Proteomics *1*, 451–465.

Ou, G., Blacque, O. E., Snow, J. J., Leroux, M. R., and Scholey, J. M. (2005a). Functional coordination of intraflagellar transport motors. Nature *436*, 583–587.

Ou, G., Qin, H., Rosenbaum, J. L., and Scholey, J. M. (2005b). The PKD protein qilin undergoes intraflagellar transport. Curr. Biol. *15*, R410–R411.

Pan, J., Wang, Q., and Snell, W. J. (2005). Cilium-generated signaling and cilia-related disorders. Lab. Invest. *85*, 452–463.

Pan, X., Ou, G., Civelekoglu-Scholey, G., Blacque, O. E., Endres, N. F., Tao, L., Mogilner, A., Leroux, M. R., Vale, R. D., and Scholey, J. M. (2006). Mechanism of transport of IFT particles in *C. elegans* cilia by the concerted action of kinesin-II and OSM-3 motors. J. Cell Biol. *174*, 1035–1045.

Pazour, G. J., Agrin, N., Leszyk, J., and Witman, G. B. (2005). Proteomic analysis of a eukaryotic cilium. J. Cell Biol. *170*, 103–113.

Pazour, G. J., Dickert, B. L., and Witman, G. B. (1999). The DHC1b (DHC2) isoform of cytoplasmic dynein is required for flagellar assembly. J. Cell Biol. *144*, 473–481.

Peckol, E. L., Zallen, J. A., Yarrow, J. C., and Bargmann, C. I. (1999). Sensory activity affects sensory axon development in *C. elegans*. Development *126*, 1891–1902.

Perens, E. A., and Shaham, S. (2005). *C. elegans* daf-6 encodes a patched-related protein required for lumen formation. Dev. Cell *8*, 893–906.

Perkins, L. A., Hedgecock, E. M., Thomson, J. N., and Culotti, J. G. (1986). Mutant sensory cilia in the nematode *Caenorhabditis elegans*. Dev. Biol. *117*, 456–487.

Piperno, G., Siuda, E., Henderson, S., Segil, M., Vaananen, H., and Sassaroli, M. (1998). Distinct mutants of retrograde intraflagellar transport (IFT) share similar morphological and molecular defects. J. Cell Biol. *143*, 1591–1601.

Porter, M. E., Bower, R., Knott, J. A., Byrd, P., and Dentler, W. (1999). Cytoplasmic dynein heavy chain 1b is required for flagellar assembly in *Chlamydomonas*. Mol. Biol. Cell *10*, 693–712.

Qin, H., Burnette, D. T., Bae, Y. K., Forscher, P., Barr, M. M., and Rosenbaum, J. L. (2005). Intraflagellar transport is required for the vectorial movement of TRPV channels in the ciliary membrane. Curr. Biol. *15*, 1695–1699.

Qin, H., Diener, D. R., Geimer, S., Cole, D. G., and Rosenbaum, J. L. (2004). Intraflagellar transport (IFT) cargo: IFT transports flagellar precursors to the tip and turnover products to the cell body. J. Cell Biol. *164*, 255–266.

Qin, H., Rosenbaum, J. L., and Barr, M. M. (2001). An autosomal recessive polycystic kidney disease gene homolog is involved in intraflagellar transport in *C. elegans* ciliated sensory neurons. Curr. Biol. *11*, 457–461.

Reese, T. S. (1965). Olfactory cilia in the frog. J. Cell Biol. *25*, 209–230.

Rosenbaum, J. L., and Witman, G. B. (2002). Intraflagellar transport. Nat. Rev. Mol. Cell Biol. *3*, 813–825.

Rothnagel, J. A., and Rogers, G. E. (1986). Trichohyalin, an intermediate filament-associated protein of the hair follicle. J. Cell Biol. *102*, 1419–1429.

Schafer, J. C., Winkelbauer, M. E., Williams, C. L., Haycraft, C. J., Desmond, R. A., and Yoder, B. K. (2006). IFTA-2 is a conserved cilia protein involved in pathways regulating longevity and dauer formation in *Caenorhabditis elegans*. J. Cell Sci. *119*, 4088–4100.

Scholey, J. M. (2003). Intraflagellar transport. Annu. Rev. Cell Dev. Biol. *19*, 423–443.

Scholey, J. M., Ou, G., Snow, J., and Gunnarson, A. (2004). Intraflagellar transport motors in *Caenorhabditis elegans* neurons. Biochem. Soc. Trans. *32*, 682–684.

Signor, D., Wedaman, K. P., Orozco, J. T., Dwyer, N. D., Bargmann, C. I., Rose, L. S., and Scholey, J. M. (1999). Role of a class DHC1b dynein in retrograde transport of IFT motors and IFT raft particles along cilia, but not dendrites, in chemosensory neurons of living *Caenorhabditis elegans*. J. Cell Biol. *147*, 519–530.

Singla, V., and Reiter, J. F. (2006). The primary cilium as the cell's antenna: signaling at a sensory organelle. Science *313*, 629–633.

Snow, J. J., Ou, G., Gunnarson, A. L., Walker, M. R., Zhou, H. M., Brust-Mascher, I., and Scholey, J. M. (2004). Two anterograde intraflagellar transport motors cooperate to build sensory cilia on *C. elegans* neurons. Nat. Cell Biol. *6*, 1109–1113.

Starich, T. A., Herman, R. K., Kari, C. K., Yeh, W. H., Schackwitz, W. S., Schuyler, M. W., Collet, J., Thomas, J. H., and Riddle, D. L. (1995). Mutations affecting the chemosensory neurons of *Caenorhabditis elegans*. Genetics *139*, 171–188.

Stoetzel, C. *et al.* (2006). BBS10 encodes a vertebrate-specific chaperonin-like protein and is a major BBS locus. Nat. Genet. *38*, 521–524.

Stoetzel, C. *et al.* (2007). Identification of a novel BBS gene (BBS12) highlights the major role of a vertebrate-specific branch of chaperonin-related proteins in Bardet-Biedl syndrome. Am. J. Hum. Genet. *80*, 1–11.

Uchida, O., Nakano, H., Koga, M., and Ohshima, Y. (2003). The *C. elegans* che-1 gene encodes a zinc finger transcription factor required for specification of the ASE chemosensory neurons. Development *130*, 1215–1224.

Ward, S., Thomson, N., White, J. G., and Brenner, S. (1975). Electron microscopical reconstruction of the anterior sensory anatomy of the nematode *Caenorhabditis elegans*. J. Comp. Neurol. *160*, 313–337.

Wicks, S. R., de Vries, C. J., van Luenen, H. G., and Plasterk, R. H. (2000). CHE-3, a cytosolic dynein heavy chain, is required for sensory cilia structure and function in *Caenorhabditis elegans*. Dev. Biol. *221*, 295–307.

Wicks, S. R., Yeh, R. T., Gish, W. R., Waterston, R. H., and Plasterk, R. H. (2001). Rapid gene mapping in *Caenorhabditis elegans* using a high density polymorphism map. Nat. Genet. *28*, 160–164.